Structural properties of the graphene-SiC(0001) interface as a key for the preparation of homogeneous large-terrace graphene surfaces

C. Riedl and U. Starke*
Max-Planck-Institut für Festkörperforschung, Heisenbergstrasse 1, D-70569 Stuttgart, Germany

J. Bernhardt, M. Franke, and K. Heinz
Lehrstuhl für Festkörperphysik, Universität Erlangen-Nürnberg, Staudtstrasse 7, D-91058 Erlangen, Germany
(Received 18 July 2007; published 7 December 2007)

We report on the interface between graphene and 4H-SiC(0001) as investigated by scanning tunneling microscopy (STM) and low energy electron diffraction (LEED). It is characterized by the so-called $(6\sqrt{3}\times 6\sqrt{3})$R30° reconstruction, whose structural properties are still controversially discussed but at the same time are crucial for the controlled growth of homogeneous high-quality large-terrace graphene surfaces. We discuss the role of three observed phases with periodicities $(6\sqrt{3}\times 6\sqrt{3})$R30°, (6×6), and (5×5). Their LEED intensity levels and spectra strongly depend on the surface preparation procedure applied. The graphitization process imprints distinct features in the STM images as well as in the LEED spectra. The latter have the potential for an easy and practicable determination of the number of graphene layers by means of LEED.

DOI: 10.1103/PhysRevB.76.245406 PACS number(s): 81.05.Uw, 68.47.Fg, 61.14.Hg, 68.37.Ef

I. INTRODUCTION

When van Bommel *et al.* investigated the graphitization of SiC(0001) for the first time in 1975,[1] it was not conceivable that 30 years later this experimental procedure would give access to purely two-dimensional crystals with their astonishing physical properties. At present, the physics of one or several graphene layers attracts tremendous interest. One single graphite layer is called graphene due to the sp^2-bonding configuration of the carbon atoms that are distributed in a hexagonal lattice. The notion of graphene is used for single layer graphene, bilayer graphene, and few-layer graphene (up to about ten layers) that all can be seen as different types of two-dimensional crystals.[2] A number of graphene layers larger than about 10 results in bulk graphite. In addition to its own interesting electronic structure, graphene represents the building block of carbon nanotubes or fullerenes. Graphene has been presumed to be thermodynamically unstable as a freestanding layer[3,4] until Novoselov *et al.* obtained graphene by micromechanical cleavage of graphite in 2004.[5] The electronic band structure of graphene shows a linear dispersion at the Fermi energy at the $\bar{K}$ point of the surface Brillouin zone instead of a parabolic relation.[6–9] The electron transport is governed by Dirac's (relativistic) equation rather than the Schrödinger equation.[2,5,10–13] Graphene has unconventional two-dimensional electron gas properties and shows quantum confinement.[2,5,10,14] Several new varieties of the quantum Hall effect have been demonstrated.[11] Graphene-based nanoelectronics as well as the analysis of (relativistic) quantum mechanical effects are the prospects of this new physical system.[2,5,10–13]

Despite the success of the micromechanical cleaving technique, the most promising approach to obtain graphene for practical electronic applications seems to be the above mentioned controlled graphitization of SiC surfaces. After its first realization, this procedure has been investigated intensively, yet mainly under the aspect of full graphitization of the surfaces.[1,15–22] Only recently, a graphene-like electronic structure was found for the initial stages developing during this procedure.[23,24] The first stage of graphitization is the $(6\sqrt{3}\times 6\sqrt{3})$R30° reconstruction whose nature has been discussed controversially.[1,15–25] Originally, it was interpreted as a surface-graphene layer.[23] However, it now seems clear that the specific properties of graphene develop only with the first layer of graphene on top of this $(6\sqrt{3}\times 6\sqrt{3})$R30° structure[7–9,25] with the interface remaining unperturbed during growth. Yet, it is still unclear under which preparation conditions homogeneous large-area graphene layers can be obtained and at what stage of the high-temperature treatment single layer or bilayers develop. The scenario may even depend on the SiC polytype. In addition, the atomic structure of the interface and of the graphene layer are unknown. This latter fact should not come as a surprise since the (1×1) unit vectors of SiC(0001) are 3.08 Å and the unit vectors of graphene are 2.46 Å long. A $(6\sqrt{3}\times 6\sqrt{3})$R30° cell has then a 32 Å side length and contains 108 Si and 108 C atoms per SiC bilayer or 338 atoms in a graphene layer.

In this work, we are concluding from low energy electron diffraction (LEED) as well as scanning tunneling microscopy (STM) experiments that the so-called $(6\sqrt{3}\times 6\sqrt{3})$R30° reconstruction comprises three periodicities that can be observed in different ways: $(6\sqrt{3}\times 6\sqrt{3})$R30°, (6×6), and (5×5). The kind of preparation procedure influences the structural properties of the graphene-4H-SiC(0001) interface. The growth of graphene layers results in distinct features in the STM images as well as in the LEED patterns. Fingerprints in the LEED intensity spectra for the graphitization process have the prospect of an easy and practicable determination of the number of graphene layers.

II. EXPERIMENT

Before loading into the ultrahigh vacuum (UHV) chamber, the Si-terminated *n*-type 4H-SiC(0001) samples were

thermally etched using ultrapure hydrogen in order to remove polishing damage. By applying this treatment, it is possible to obtain a regular array of atomically flat terraces as well as to chemically passivate the surface.[26] Three different procedures were used for the *in situ* graphitization in the UHV chamber.

(A) After annealing the sample at 800 °C in a Si flux ($\approx$1 ML/min), the Si-rich (3×3) reconstruction[27] develops. Without further Si addition, this structure is used as the starting point for the preparation of graphene layers on SiC(0001).[18,21] The C-rich $(6\sqrt{3}\times6\sqrt{3})$R30° reconstruction can then be obtained by heating directly up to 1250 °C. Alternatively, a further annealing step at 1000 °C can be added, leading to the $(\sqrt{3}\times\sqrt{3})$R30° structure which is still covered by Si adatoms.[28] Between 1100 and 1200 °C, the $(6\sqrt{3}\times6\sqrt{3})$R30° reconstruction begins to develop but coexists with the $(\sqrt{3}\times\sqrt{3})$R30° structure. The pure $(6\sqrt{3}\times6\sqrt{3})$R30° reconstruction is accomplished between 1200 and 1300 °C. Further annealing above 1300–1350 °C leads to the growth of graphene layers on top of this structure whereby the $(6\sqrt{3}\times6\sqrt{3})$R30° periodicity is retained. Heating was conducted by electron bombardment with each annealing step taking about 15 min. An electron beam evaporator was used for Si evaporation and the temperatures were determined by a pyrometer.

(B) After initially annealing the sample at 950 °C in a flux of Si ($\approx$1 ML/min), the $(\sqrt{3}\times\sqrt{3})$R30° structure develops. By further heating of this surface without further Si addition, the desired level of graphitization could be realized.

(C) Annealing of the *ex situ* prepared silicate $(\sqrt{3}\times\sqrt{3})$R30° reconstruction that develops during the hydrogen etching procedure[29] immediately leads to the $(6\sqrt{3}\times6\sqrt{3})$R30° phase.

The results of the different graphitization steps were analyzed using a four grid back view LEED optics and a Besocke-type scanning tunneling microscope. The surface morphology was determined by atomic force microscopy (AFM) under ambient conditions after removing the sample from the UHV chamber.

III. $(6\sqrt{3}\times6\sqrt{3})$R30° PHASE AS A PRECURSOR OF GRAPHITIZATION

Figure 1 displays LEED patterns of the coexisting $(\sqrt{3}\times\sqrt{3})$R30° and $(6\sqrt{3}\times6\sqrt{3})$R30° reconstructions of 4H-SiC(0001) corresponding to the above described preparation procedures A, B, and C and after the sample had been annealed at around 1200 °C. All three patterns are usually interpreted as having a $(6\sqrt{3}\times6\sqrt{3})$R30° periodicity. Yet, a detailed inspection of the spots in the vicinity of the $\frac{1}{3}$ diffraction order as displayed in the enlarged sections on the right of the three LEED patterns (shown both in normal and reverse contrast for clarity) reveals a more complex scenario. The spot indicated by the arrow in the reverse contrast image is at the $(\frac{1}{3},\frac{1}{3})$ position which is characteristic for the $(\sqrt{3}\times\sqrt{3})$R30° structure. It gradually disappears with increasing temperature as the corresponding domains disappear, too. The spots on the triangle marked in green (light gray) have

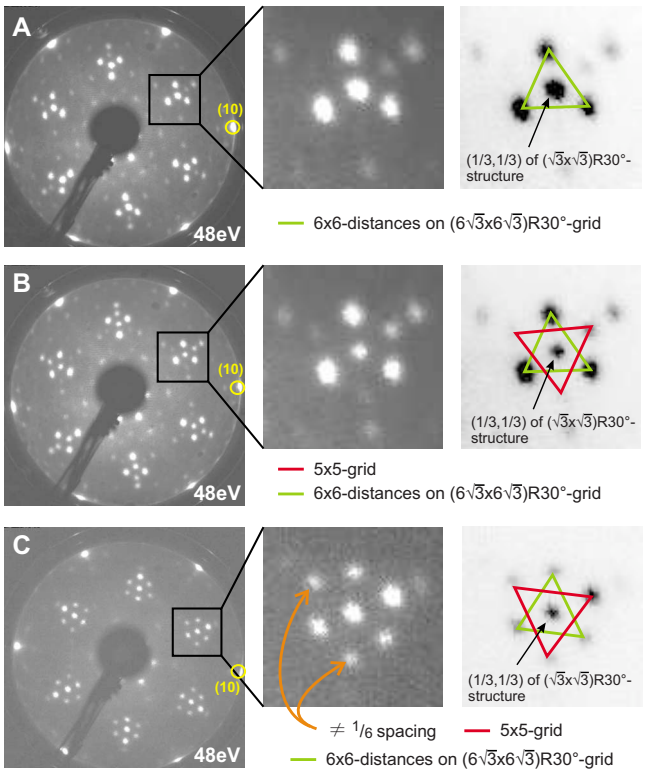

FIG. 1. (Color online) LEED patterns of the mixed $(\sqrt{3}\times\sqrt{3})$R30° and $(6\sqrt{3}\times6\sqrt{3})$R30° reconstruction of 4H-SiC(0001) for three different preparation procedures labeled A, B, and C (see text for details), after annealing at a temperature of about 1200 °C. Using procedure A, the Si-rich (3×3) structure is annealed, using procedure B, the $(\sqrt{3}\times\sqrt{3})$R30° structure is heated up, and during procedure C, the preparation is conducted by annealing an *ex situ* sample. Spots on a $(6\sqrt{3}\times6\sqrt{3})$R30° grid as well as on a (5×5) grid can be observed exhibiting different relative intensities.

distances of $\frac{1}{6}$ of the substrate's reciprocal surface unit-mesh vector. However, since the $(\frac{1}{3},\frac{1}{3})$ position in the center of the triangle is part of a (6×6) grid on the SiC(0001) surface, it is clear that the spots on the green (light gray) triangle are shifted with respect to the (6×6) grid and belong to a true $(6\sqrt{3}\times6\sqrt{3})$R30° grid. It has to be emphasized that this $(6\sqrt{3}\times6\sqrt{3})$R30° reconstruction indeed has its designated periodicity. It is not of (6×6) periodicity which could be assumed from the (6×6) corrugations that can be observed in STM (see below). The fact that not all diffraction spots on the $(6\sqrt{3}\times6\sqrt{3})$R30° grid are visible can be attributed to kinematic suppression. However, in addition, diffraction spots can be observed that are not precisely positioned on the $(6\sqrt{3}\times6\sqrt{3})$R30° grid, namely, the spots indicated by the triangles marked in red (dark gray) in the case of preparation procedures B and C. These spots have a larger distance than the spots on the green (light gray) triangle and thus cannot belong to the $(6\sqrt{3}\times6\sqrt{3})$R30° grid. They rather have to be attributed to a (5×5) grid as was confirmed from LEED data at different energies. Due to small distortions of the LEED screen or deviations of the sample from the centric position, both triangles [red (dark gray) and green (light gray)] are not precisely equilateral. Of course, spots at different diffraction

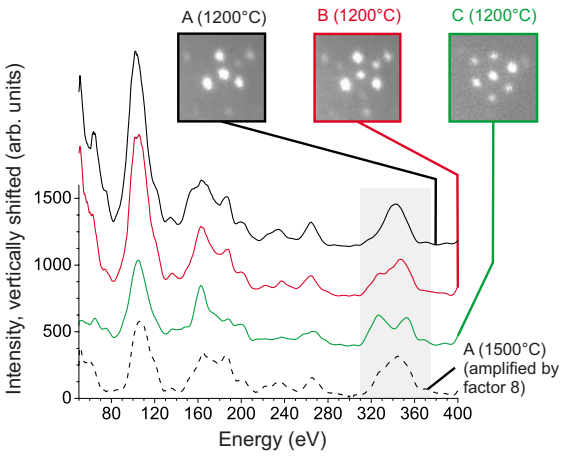

FIG. 2. (Color online) Preparation dependent LEED intensity spectra of the (10) spots of the $(6\sqrt{3}\times 6\sqrt{3})$R30° reconstruction in the state after annealing at about 1200 °C, where the $(\frac{1}{3},\frac{1}{3})$ spots from the $(\sqrt{3}\times\sqrt{3})$R30° structure are still visible. During preparation procedure A, the Si-rich (3×3) structure is annealed, during preparation procedure B, the $(\sqrt{3}\times\sqrt{3})$R30° reconstruction is heated up, and during procedure C, the preparation is conducted by annealing an *ex situ* sample. In addition, the (10) spectrum is shown after full graphitization at 1500 °C (dashed curve).

orders on the (5×5) grid have different intensities, due to multiple scattering. The absolute intensities of the spots on the (5×5) grid are different for the different preparation procedures, and for preparation procedure A, they even seem too faint to deduce the existence of (5×5) domains at the surface. However, the relative spot intensities on the red triangle are equal, indicating the origin from the same kind of surface structure within the (5×5) domains. With respect to the preparation of graphene surfaces, it can be concluded that details of the preparation procedure applied during the development of the intermediate $(6\sqrt{3}\times 6\sqrt{3})$R30° phase can strongly influence their quality as well as the atomic arrangement at the surface. This can be verified by inspection of the LEED spot intensities: a different arrangement of the atoms at the surface results in different multiple scattering pathways in LEED and therefore affects the intensities of the SiC-substrate spots as a function of the energy, i.e., yields different $I(E)$ spectra. Indeed, Fig. 2 exhibits that the three applied preparation procedures lead to characteristic differences in the $I(E)$ spectra of the $(6\sqrt{3}\times 6\sqrt{3})$R30° reconstruction in the state after annealing at about 1200 °C where the $(\frac{1}{3},\frac{1}{3})$ spots from the $(\sqrt{3}\times\sqrt{3})$R30° structure are still visible. The differences are most prominent in the energy range 320–370 eV. While the absolute intensity level is less important, the energy positions of the peaks and minima play the crucial role.[30] Starting the preparation of the $(6\sqrt{3}\times 6\sqrt{3})$R30° reconstruction from the (3×3) phase (procedure A) results in a single peak at 342 eV in the SiC-substrate spot intensity, whereas a double peak structure appears at 328 and 347 eV when using the $(\sqrt{3}\times\sqrt{3})$R30° reconstruction as the starting point (procedure B). Annealing of the *ex situ* silicate $(\sqrt{3}\times\sqrt{3})$R30° phase leads to two well resolved peaks at 326 and 352 eV. A quite similar behavior was observed previously for the preparation of the $(\sqrt{3}\times\sqrt{3})$R30° reconstruction using 4H- and 6H-SiC(0001).[28,31] In that case, it was concluded from a quantitative LEED structure analysis that annealing of the *ex situ* sample does not change the number of equally oriented bilayers at the surface, i.e., two for 4H-SiC(0001) ("S2 termination") and three for 6H-SiC(0001) ("S3 termination"). Astonishingly, however, the S3 termination develops for both 4H- and 6H-SiC(0001) after annealing of the (3×3) reconstruction, which actually implies that the bulk stacking sequence is broken in the case of 4H-SiC(0001). But why should this be important for the growth of graphene layers on top of the $(6\sqrt{3}\times 6\sqrt{3})$R30° reconstruction? First, it is clear that three SiC bilayers are necessary to grow one graphene layer from a simple count of the carbon atoms. Hence, the S3 termination should provide a better precondition for a homogeneous graphene development than the S2 termination, so that starting the preparation from the (3×3) phase promises to be the best preparation procedure at least for 4H-SiC(0001). Second, the $I(E)$ spectra observed for the $(6\sqrt{3}\times 6\sqrt{3})$R30° phase (shown in Fig. 2) are indeed very similar to the spectra obtained from a $(\sqrt{3}\times\sqrt{3})$R30° phase.[31] Even after full graphitization at $T\approx 1500$ °C, the spectrum is hardly changed (Fig. 2). The intensity, however, is strongly reduced, indicating that the signal is attenuated by layers above or that the signal comes only from a small fraction of the surface. It is rather astonishing that the graphitization process does not influence the position of the maxima and minima in the $I(E)$ spectra. At least one might expect significant changes in the energy range between 320 and 360 eV as the S3-terminated SiC bilayers should have been used up completely during graphitization and should leave behind S2-terminated SiC bilayers beneath the graphene layers provided the stacking rearrangement is not repeated during the graphitization process. In this respect, the need for a structure determination, e.g., by means of quantitative LEED, is quite obvious.

The role of the (5×5) periodicity in the different preparation procedures can be elucidated using STM. Figure 3(a) shows a filled state STM image of the $(6\sqrt{3}\times 6\sqrt{3})$R30° reconstruction exhibiting two different periodicities, a (6×6) honeycomb structure on the left side and a (5×5) structure on the right side of the panel. The (5×5) structure is characterized by clusters with a varying number of atoms. We observe this structure for all three preparation procedures independent of the annealing temperature of the $(6\sqrt{3}\times 6\sqrt{3})$R30° reconstruction. The number and fraction of (5×5) domains, however, are larger for the *ex situ* prepared sample (procedure C), in full agreement with the stronger intensity level of the (5×5) LEED spots. In our STM measurements, this (5×5) structure can be seen only rather rarely. Furthermore, the surface quality of the annealed *ex situ* sample is not good enough to obtain a large number of STM images producing good statistics. A (5×5) reconstruction found in LEED and STM was also previously reported in the framework of the $(6\sqrt{3}\times 6\sqrt{3})$R30° phase.[15] In that case, an *ex situ* sample was annealed without simultaneous Si deposition. The fact that there have been no further reports on a (5×5) reconstruction recently might be due to the circumstance that, during the last years, it has become quite

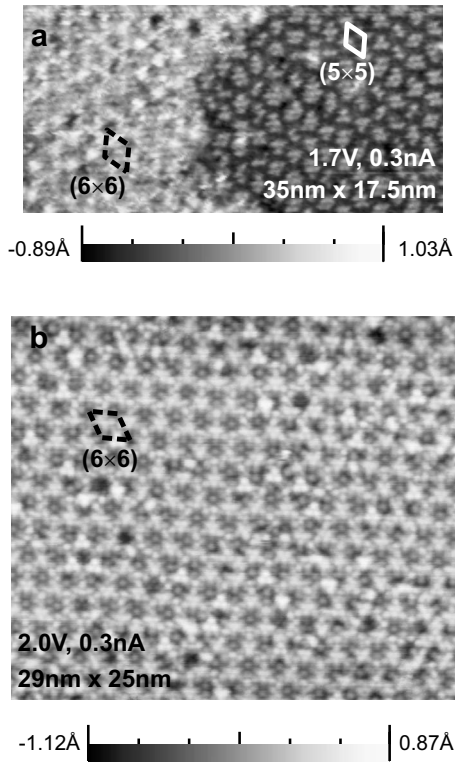

FIG. 3. Typical STM images of the $(6\sqrt{3}\times6\sqrt{3})$R30° on 4H-SiC(0001) mainly show (6×6) corrugations [panel (b) and left side of panel (a)] but sometimes also (5×5) corrugations [right side of panel (a)]. The latter are responsible for the deviations from the $(6\sqrt{3}\times6\sqrt{3})$R30° periodicity in the LEED patterns shown in Fig. 1.

common to use Si deposition in the preparation procedure. Nevertheless, some (5×5) patches are present also when starting the preparation from the Si-rich (3×3) phase.

Figure 3(b) shows the filled states of the apparent (6×6) periodicity in more detail. The image demonstrates the complexity of the reconstruction. Different apparent features can be seen that lack an obvious long-range order. Inside the honeycomb rings, a different number of atoms with a different arrangement of the atoms is observed. The atomic and electronic structure of this reconstruction is not well understood up to now. The structural appearance of the $(6\sqrt{3}\times6\sqrt{3})$R30° phase strongly depends on the tunneling voltage. The (6×6) periodicity is mainly pronounced at high tunneling bias, whereas at low bias it is difficult to observe a clear long-range periodicity. Using such small tunneling voltages, however, one can possibly resolve the true $(6\sqrt{3}\times6\sqrt{3})$R30° structure as shown in Fig. 4. Panel (a) shows a STM image at 1.7 V bias still exhibiting corrugations with (6×6) periodicity. Further reduction of the tunneling voltage down to 0.2 V reveals two types of rings with slightly different sizes, thus forming a unit cell larger than that of the (6×6) periodicity [panel (b)], namely, a unit cell of $(6\sqrt{3}\times6\sqrt{3})$R30° periodicity. Three atomic bumps within the rings are only present in the larger rings. Each bump is part of a diamond of four atoms [marked in red (dark gray) in panel (b)] which — in the same orientation — is repeated only with the $(6\sqrt{3}\times6\sqrt{3})$R30° periodicity. This is elucidated in panels (b) and (c) of Fig. 4 by a sketch of the rings with their different sizes and the three additional atoms (or atomic clusters). The lower part of panel (b) displays the same surface area as the upper part. The unit cells of the (6×6) and the $(6\sqrt{3}\times6\sqrt{3})$R30° periodicity are indicated in panel (c). With this real space arrangement, the periodicity of the LEED patterns can be explained, which is not possible assuming a (6×6) structure only.

However, this very complex structure is only partially resolved up to now. In the literature, several models exist that do not consider the $(6\sqrt{3}\times6\sqrt{3})$R30° structure as an inherent surface reconstruction of SiC(0001). Mårtensson *et al.* proposed the coexistence of a (6×6) and an incommensurate $(\sqrt{2.1}\times\sqrt{2.1})$R30° phase,[15] which is not in agreement with the interpretation of our LEED and STM results. It has often been argued that the LEED diffraction image shows a moiré pattern of graphite and the SiC substrate [(1×1) (Refs. 1 and 23) or $(\sqrt{3}\times\sqrt{3})$R30° (Ref. 19)]. However, such an interpretation is in inconsistency with both band structure measurements using angular resolved photoelectron spectroscopy (ARPES)[7–9] and the STM image displayed in Fig. 4. Furthermore, STM images show that graphene is growing on top of the $(6\sqrt{3}\times6\sqrt{3})$R30° reconstruction (see Fig. 7 below). The specific properties of graphene develop only with the first layer of graphite on top of the $(6\sqrt{3}\times6\sqrt{3})$R30° structure,[7–9,25] while the latter remains unperturbed during

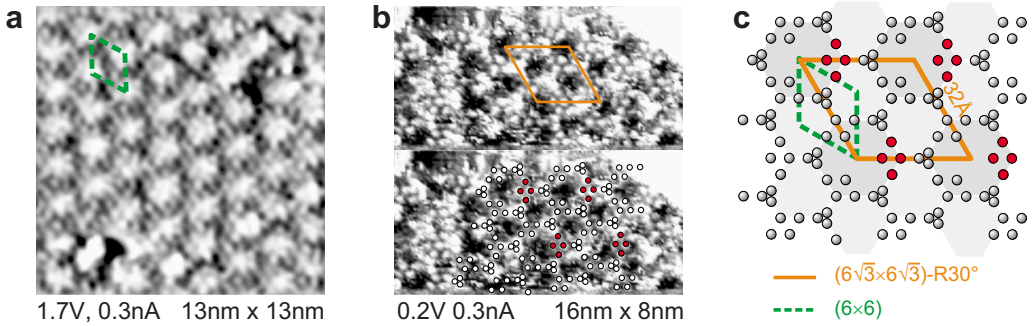

FIG. 4. (Color online) Atomically resolved STM images at U_{tip}=1.7 V [panel (a)] and U_{tip}=0.2 V [panel (b)]. Whereas panel (a) shows (6×6) corrugations, panel (b) exhibits rings of adatoms of two different sizes, thus leading to a $(6\sqrt{3}\times6\sqrt{3})$R30° unit cell. The lower part of panel (b) displays the same surface area as the upper part and shows a sketch of the rings with their different sizes. The arrangement of the atoms or atomic clusters together with the corresponding unit cells is displayed in panel (c).

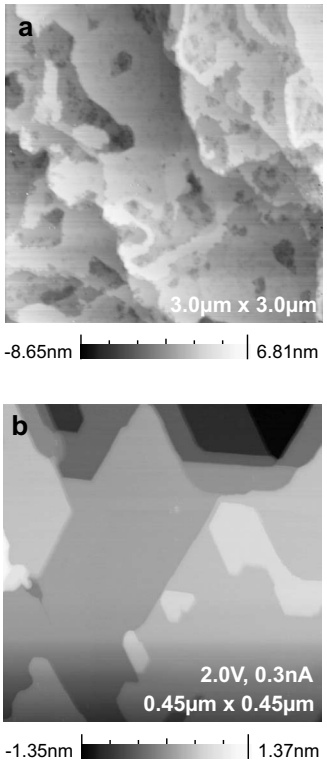

FIG. 5. Panel (a) shows a typical AFM image of the $(6\sqrt{3}\times 6\sqrt{3})$R30° reconstruction before the graphitization process, whereas panel (b) shows a large-area STM image after graphitization. The maximum terrace size amounts to a few hundreds of nm^2.

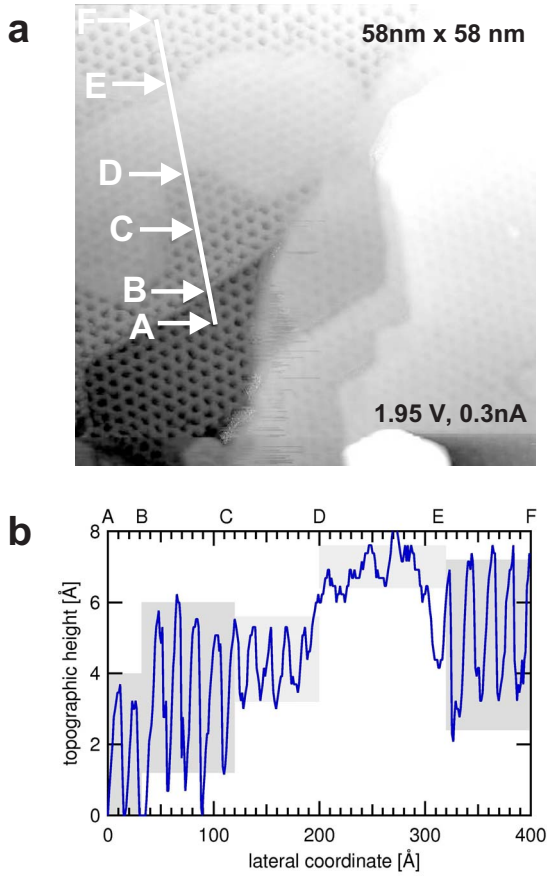

FIG. 6. (Color online) STM image of the $(6\sqrt{3}\times 6\sqrt{3})$R30° reconstruction on 4H-SiC(0001) showing terraces with different corrugation due to a different number of graphene layers on top of the $(6\sqrt{3}\times 6\sqrt{3})$R30° reconstruction.

the growth of the graphene layers. A recently proposed model by Chen *et al.* suggests a self-organization of surface carbon atoms in a "carbon nanomesh" with (6×6) periodicity.[22] This model is also in contradiction to the band structure measurements. Furthermore, it is claimed that the STM images look the same for different tunneling voltages. Our STM images clearly show different atomic orbitals of the structure for different bias voltages, which is in accordance with earlier observations.[15]

In order to underline the importance of an understanding of the graphene-SiC(0001) interface for the controlled growth of large-terrace graphene surfaces, we show in Fig. 5 an AFM image of the $(6\sqrt{3}\times 6\sqrt{3})$R30° reconstruction before the graphitization process [panel (a)] and a large-area STM image after graphitization [panel (b)]. The typical length scale of the surface morphology appears to be determined already in the state of the $(6\sqrt{3}\times 6\sqrt{3})$R30° reconstruction. Terrace sizes up to several hundred nm^2 can be obtained but it would be desirable to let graphene grow in even larger regions. The AFM and STM images show a lot of small terraces where the growth conditions seem to be different so that, for instance, a different number of graphene layers may develop or linear defects of the graphene layer are present as a consequence of substrate steps. So far, no preparation procedure exists that produces substantially larger homogeneous graphene surfaces (compare STM image in Ref. 24 and AFM images in Refs. 7 and 32). It should be noted that after the initial hydrogen etch process, the surface exhibits regular terraces with straight step edges of typically micrometer distance.

IV. GRAPHITIZATION PROCESS

In this section, we analyze the graphitization process of SiC(0001) by means of LEED and STM starting with the $(6\sqrt{3}\times 6\sqrt{3})$R30° reconstruction prepared by annealing of the (3×3) structure (procedure A in the previous sections). Figure 6 shows STM measurements after graphitization using a bias where the apparent (6×6) corrugation can be observed best. Clearly, the development of homogeneous graphene layers on top of the $(6\sqrt{3}\times 6\sqrt{3})$R30° structure seems to be prevented. As illustrated in the STM image in panel (a), different terraces display a different corrugation of the (6×6) honeycomb lattice. This can be seen more clearly in the quantitative line scan in panel (b). For reference, note that the vertical spacing of bulk SiC bilayers amounts to 2.52 Å and that the layer spacing in (bulk) graphite is 3.35 Å. At the point labeled B, one substrate bilayer step can be observed. Regions [AC] and [EF] have the same large corrugation, whereas the height of the corrugation of region [CD] amounts to half of the former value. Along section [DE], the corrugation is even further reduced to about one-

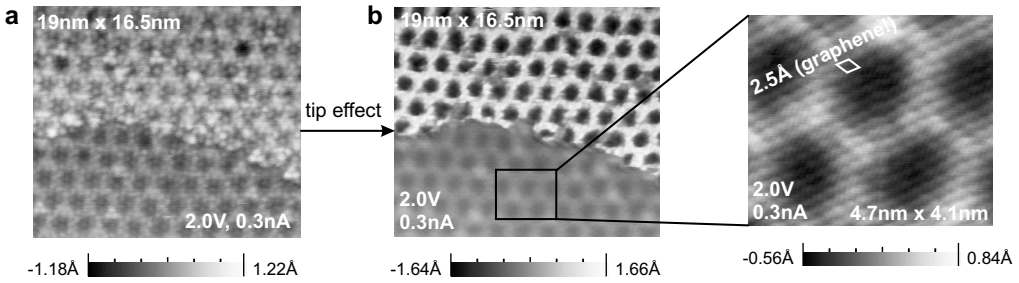

FIG. 7. Atomically resolved STM images of the $(6\sqrt{3}\times 6\sqrt{3})$R30° reconstruction on 4H-SiC(0001) showing (6×6) corrugations with two different contrasts for two different tip conditions shown in panels (a) and (b). Only for the tip condition in panel (b) can graphene on top of the $(6\sqrt{3}\times 6\sqrt{3})$R30° reconstruction be resolved (lower part of the STM image). The annealing temperature was around 1300 °C.

fourth of the [AC] value. These effects can be interpreted to be caused by a different number of graphene layers on top of the $(6\sqrt{3}\times 6\sqrt{3})$R30° surface reconstruction and it appears that electronic effects completely cover topographical effects in the STM height measurements. Regions [BC] and [EF] clearly resemble similar surface structures at the same height level as can be drawn from comparing the step heights in a line profile taken slightly to the right (not shown). Their residual intensity difference should be attributed to a slight tilt in the line scan. In Fig. 7, we show that graphene layers not only can be seen indirectly by means of a contrast change but can also directly be identified. The annealing temperature in that case was around 1300 °C. For two different tip conditions, we compare the images of the same surface area that contrast differently on the corresponding terraces. The first tip condition allows for atomic resolution of the $(6\sqrt{3}\times 6\sqrt{3})$R30° reconstruction, whereas the second one seems to allow only for a reduced quality at a first glance. However, scaling down the scanning area leads to atomic resolution of graphene on top of the $(6\sqrt{3}\times 6\sqrt{3})$R30° surface reconstruction. Yet, this is only the case for the region with the reduced contrast. The unit-cell size of about 2.5 Å corresponds to that of graphite. Yet, since we observe only one of the two carbon atoms comprising the graphene unit cell, we identify this surface region as (at least) bilayer graphene. The Bernal stacking of two graphene sheets leads to the observation of such a diamond-shaped lattice.[33] The crucial point that should be emphasized is that the visibility of the graphene layers strongly depends on the actual tip condition, thus complicating the determination of the number of graphene layers by means of STM. In the upper part of Fig. 7, the higher contrast in the STM image represents a lower coverage with graphene, possibly no graphene layer at all. However, it cannot be ruled out that a single graphene layer might possibly be identified using a different bias voltage.

Up to now, it is not clear how a certain number of graphene layers can be grown on top of SiC(0001) in a definite and controlled way. Present experimental statements about the number of graphene layers in a large area (e.g., on a 100 μm scale) are carried out by ARPES,[7–9] Auger electron spectroscopy (AES),[23,24,32] x-ray photoelectron spectroscopy (XPS), or LEED. The diameter of the probing beam of these methods is much larger than the terrace size with a definite number of graphene layers so that always an average value is obtained. The reliability of using the Si/C intensity ratio in AES or XPS also suffers from the inaccurate knowledge of the inelastic attenuation of the electrons probing the surface. Raman spectroscopy offers a much smaller beam diameter than the other techniques mentioned. Also, it has already been used successfully to identify graphene layers obtained by micromechanical cleavage.[34] Yet, it would be desirable to find an easy and exact way for the determination of the number of graphene layers that can be used in the home laboratory and, in particular, continuously during the preparation procedure. We show that LEED intensity spectra, which can be obtained in the same UHV chamber, have the potential to be used as fingerprints and so offer a solution to this problem. During graphitization, the LEED pattern continuously undergoes variations visible by eye [see Fig. 8; the inset above the $I(E)$ spectra indicates the spots being discussed in this context]: in the first stage, the $(6\sqrt{3}\times 6\sqrt{3})$R30° reconstruction coexists with the $(\sqrt{3}\times\sqrt{3})$R30° phase as noted before (scenario at 1210 °C). Higher temperatures (approximately 1280 °C) lead to the disappearance of the spots related to the $(\sqrt{3}\times\sqrt{3})$R30° structure, i.e., the diffraction spots at the $(\frac{1}{3},\frac{1}{3})$ position and at the $(\frac{2}{3},\frac{2}{3})$ position. When graphene layers are growing on top of this pure $(6\sqrt{3}\times 6\sqrt{3})$R30° structure (above 1300 °C), a LEED spot with a distance that is related to that of bulk graphite (about 2.5 Å) shows an increasing intensity. Simultaneously, the diffuse background in the LEED patterns continuously increases. Nevertheless, STM images still show a similar surface quality as shown above for the pure $(6\sqrt{3}\times 6\sqrt{3})$R30° reconstruction. The graphite related spot is positioned next to the $(\frac{2}{3},\frac{2}{3})$ spot position with a $1/(6\sqrt{3})$ distance [green (light gray) dot in the inset of Fig. 8]. It has to be pointed out that this LEED spot already belongs to the $(6\sqrt{3}\times 6\sqrt{3})$R30° reconstruction and can be observed when not yet any graphene layers have grown. We have analyzed the energy dependent intensity of all clearly visible LEED spots of the $(6\sqrt{3}\times 6\sqrt{3})$R30° pattern dependent on the annealing temperature. Despite the different scattering properties for a different stage of graphitization, the LEED spectra do not show any significant changes for all diffraction spots except for the mentioned one which is characteristic for the lattice parameter of bulk graphite. The corresponding spectra are shown in Fig. 8. Significant changes in the peak shape and peak position can be seen and are highlighted. According to the STM image in Fig. 7 and according to ARPES measurements,[9] the first graphene layers develop at around 1300 °C. Bulk-like

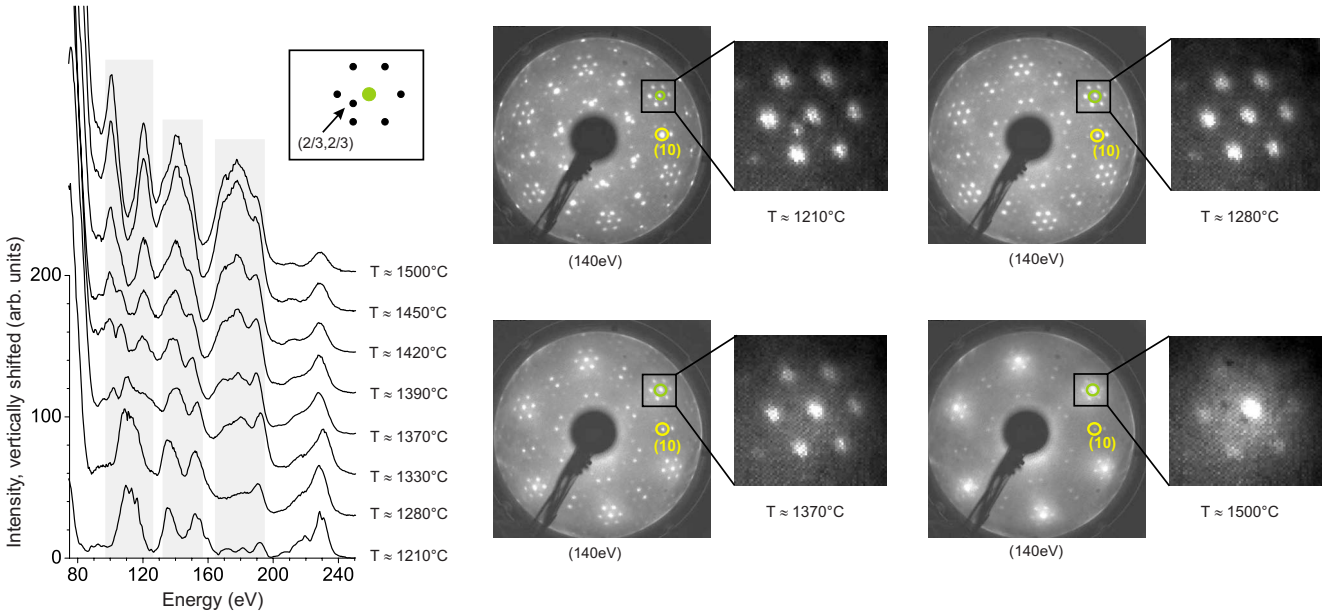

FIG. 8. (Color online) LEED intensity spectra dependent on the annealing temperature of the LEED spot marked in green (light gray) in the inset. The spectra may be used as fingerprints for an easy and practicable determination of the number of graphene layers on top of the $(6\sqrt{3}\times 6\sqrt{3})$R30° reconstruction.

graphite, i.e., around ten graphene layers or more, is obtained for temperatures increasing 1450 °C. Thus, the observed changes in the LEED intensities cover the entire graphene growth regime from a monolayer to bulk-like films and have the potential to be used to identify the graphene thickness. The upcoming task is to exactly correlate the LEED spectra characteristics with a certain number of graphene layers. This will be achieved by acquiring the LEED fingerprints in an *in situ* combined experiment with the band structure from ARPES, where the identification of the number of layers seems possible.[9] In parallel, we attempt a direct structural correlation by a quantitative LEED analysis, which may not resolve the complete surface structure but might give partial insight into the structural development of the surface before and during the graphitization process, in particular, the graphene thickness, and thus help define more precise preparation conditions.

V. CONCLUSION

STM and LEED were used to investigate the structural properties of the graphene-4H-SiC(0001) interface for several preparation procedures and for different stages of graphitization. The precursor phase of graphitization — which not yet exhibits the typical properties of graphene — is the so-called $(6\sqrt{3}\times 6\sqrt{3})$R30° reconstruction. Besides the latter, the LEED pattern also shows a (5×5) periodicity that can be observed in STM, too. The detailed nature of the preparation procedure applied significantly influences the intensity level of the (5×5) spots and the energy dependence of the SiC-substrate spots. Scanning tunneling microscopy often shows a (6×6) corrugation, but using small tunneling voltages, the true $(6\sqrt{3}\times 6\sqrt{3})$R30° structure can be revealed (at least partially). Graphene layers on top of the $(6\sqrt{3}\times 6\sqrt{3})$R30° reconstruction lead to a decreased contrast in the STM images. Under certain tip conditions, the graphene unit cell can directly be observed. The graphitization process results in significant changes in the LEED intensity spectra. As a consequence, these intensities may be used as fingerprints, providing an alternative method for the determination of the number of graphene layers (besides the approach of band structure measurements by ARPES at a synchrotron). At present, the extent to which the growth of large-terrace graphene surfaces can be controlled and realized is unknown. Further analysis of the structural properties of the graphene-SiC(0001) interface such as the application of quantitative LEED might lead to preparation procedures that make this material even more attractive for physical and industrial applications.

*u.starke@fkf.mpg.de; http://www.fkf.mpg.de/ga

[1] A. J. van Bommel, J. E. Crombeen, and A. van Tooren, Surf. Sci. **48**, 463 (1975).
[2] A. K. Geim and K. S. Novoselov, Nat. Mater. **6**, 183 (2007).
[3] R. E. Peierls, Ann. Inst. Henri Poincare **5**, 177 (1935).
[4] L. D. Landau, Phys. Z. Sowjetunion **11**, 26 (1937).
[5] K. S. Novoselov, A. K. Geim, S. V. Morozov, D. Jiang, Y. Zhang, S. V. Dubonos, I. V. Grigorieva, and A. A. Firsov, Science **306**, 666 (2004).
[6] P. R. Wallace, Phys. Rev. **71**, 622 (1947).
[7] Th. Seyller, K. V. Emtsev, K. Gao, F. Speck, L. Ley, A. Tadich, L. Broekman, J. D. Riley, R. C. G. Leckey, O. Rader, A. Varykhalov, and A. M. Shikin, Surf. Sci. **600**, 3906 (2006).
[8] T. Ohta, A. Bostwick, Th. Seyller, K. Horn, and E. Rotenberg, Science **313**, 951 (2006).
[9] K. V. Emtsev, Th. Seyller, F. Speck, L. Ley, P. Stojanov, J. D. Riley, and R. G. C. Leckey, Mater. Sci. Forum **556-557**, 525 (2006).
[10] K. S. Novoselov, A. K. Geim, S. V. Morozov, D. Jiang, M. I. Katsnelson, I. V. Grigorieva, S. V. Dubonos, and A. A. Firsov, Nature (London) **438**, 197 (2005).
[11] K. S. Novoselov, E. McCann, S. V. Morozov, V. I. Fal'ko, M. I. Katsnelson, U. Zeitler, D. Jiang, F. Schedin, and A. K. Geim, Nat. Phys. **2**, 177 (2006).
[12] M. I. Katsnelson, K. S. Novoselov, and A. K. Geim, Nat. Phys. **2**, 620 (2006).
[13] M. I. Katsnelson and K. S. Novoselov, Solid State Commun. **143**, 3 (2007).
[14] G. W. Semenoff, Phys. Rev. Lett. **53**, 2449 (1984).
[15] P. Mårtensson, F. Owman, and L. I. Johansson, Phys. Status Solidi B **202**, 501 (1997).
[16] U. Starke, J. Schardt, and M. Franke, Appl. Phys. A: Mater. Sci. Process. **65**, 587 (1997).
[17] U. Starke, M. Franke, J. Bernhardt, J. Schardt, K. Reuter, and K. Heinz, Mater. Sci. Forum **264-268**, 321 (1998).
[18] I. Forbeaux, J.-M. Themlin, and J.-M. Debever, Phys. Rev. B **58**, 16396 (1998).
[19] L. Simon, J. L. Bischoff, and L. Kubler, Phys. Rev. B **60**, 11653 (1999).
[20] A. Charrier, A. Coati, T. Argunova, F. Thibaudau, Y. Garreau, R. Pinchaux, I. Forbeaux, J.-M. Debever, M. Sauvage-Simkin, and J.-M. Themlin, J. Appl. Phys. **92**, 2479 (2002).
[21] U. Starke, in *Silicon Carbide, Recent Major Advances*, edited by W. J. Choyke, H. Matsunami, and G. Pensl (Springer, Berlin, 2004), pp. 281–316.
[22] W. Chen, H. Xu, L. Liu, X. Gao, D. Qi, G. Peng, S. C. Tan, Y. Feng, K. P. Loh, and A. T. S. Wee, Surf. Sci. **596**, 176 (2005).
[23] C. Berger, Z. Song, X. Li, X. Wu, N. Brown, C. Naud, D. Mayou, T. Li, J. Hass, A. N. Marchenkov, E. H. Conrad, P. N. First, and W. A. de Heer, Science **312**, 1191 (2006).
[24] W. A. de Heer, C. Berger, X. Wu, P. N. First, E. H. Conrad, X. Li, T. Li, M. Sprinkle, J. Hass, M. L. Sadowski, M. Potemski, and G. Martinez, Solid State Commun. **143**, 92 (2007).
[25] A. Mattausch and O. Pankratov, Phys. Rev. Lett. **99**, 076802 (2007).
[26] S. Soubatch, S. E. Saddow, S. P. Rao, W. Y. Lee, M. Konuma, and U. Starke, Mater. Sci. Forum **483-485**, 761 (2005).
[27] U. Starke, J. Schardt, J. Bernhardt, M. Franke, K. Reuter, H. Wedler, K. Heinz, J. Furthmüller, P. Käckell, and F. Bechstedt, Phys. Rev. Lett. **80**, 758 (1998).
[28] U. Starke, J. Schardt, J. Bernhardt, M. Franke, and K. Heinz, Phys. Rev. Lett. **82**, 2107 (1999).
[29] J. Bernhardt, J. Schardt, U. Starke, and K. Heinz, Appl. Phys. Lett. **74**, 1084 (1999).
[30] K. Heinz, Rep. Prog. Phys. **58**, 637 (1995).
[31] U. Starke, J. Bernhardt, J. Schardt, A. Seubert, and K. Heinz, Mater. Sci. Forum **457-460**, 415 (2004).
[32] G. Gu, S. Nie, R. M. Feenstra, R. P. Devaty, W. J. Choyke, W. K. Chan, and M. G. Kane, Appl. Phys. Lett. **90**, 253507 (2007).
[33] E. Stolyarova, K. T. Rim, S. Ryu, J. Maultzsch, P. Kim, L. E. Brus, T. F. Heinz, M. S. Hybertsen, and G. W. Flynn, Proc. Natl. Acad. Sci. U.S.A. **104**, 9209 (2007).
[34] A. C. Ferrari, J. C. Meyer, V. Scardaci, C. Casiraghi, M. Lazzeri, F. Mauri, S. Piscanec, D. Jiang, K. S. Novoselov, S. Roth, and A. K. Geim, Phys. Rev. Lett. **97**, 187401 (2006).